Research Square

Preprints are preliminary reports that have not undergone peer review.
They should not be considered conclusive, used to inform clinical practice,
or referenced by the media as validated information.

One-Pot In-Situ Growth of Dendritic Gold Nanoforests on Flexible Cellulose Paper for SERS Sensing

Vo Thi Nhat Linh

linhvtn8@fe.edu.vn

FPT University

Muhammad Shalahuddin Al Ja'farawy

University of Duisburg-Essen

Ho Sang Jung

Korea University

Research Article

Keywords: Cellulose paper, Gold nanostructures, Flexible sensor, Surface-enhance Raman scattering

Posted Date: November 17th, 2026

DOI: https://doi.org/10.21203/rs.3.rs-11398220/v1

License: This work is licensed under a Creative Commons Attribution 4.0 International License.
Read Full License

Additional Declarations: No competing interests reported.

One-Pot In-Situ Growth of Dendritic Gold Nanoforests on Flexible Cellulose Paper for SERS Sensing

Vo Thi Nhat Linh[a*], Muhammad Shalahuddin Al Ja'farawy[b], and Ho Sang Jung[c*]

[a]*Faculty of Semiconductor IC and Automotive Software, FPT University, Ho Chi Minh, Vietnam*

[b]*Department of Chemistry, University of Duisburg-Essen, Essen, 45141, Germany*

[c]*School of Biomedical Engineering, Korea University, Seoul, 02841, Republic of Korea*

[*]Corresponding author

E-mail addresses: linhvtn8@fe.edu.vn (Dr. Vo Thi Nhat Linh); jhs0626@korea.ac.kr (Dr. Prof. Ho Sang Jung)

Abstract

Dendritic plasmonic nanostructures provide dense electromagnetic “hot spots” for surface-enhanced Raman scattering (SERS), but conventional wet-chemical routes typically require multistep procedures, elevated temperatures, or structure-directing surfactants that limit their integration with flexible, low-cost substrates. Here, we report a one-pot, in-situ growth of dendritic gold nanoforests (AuNFs) directly grown on cellulose paper (denoted DGP), offering a simple yet effective strategy to produce highly active, flexible, and scalable SERS substrates. Highly branching with multi-protrusions, densely formed on paper surface was observed, producing a dense, three-dimensional forest-like architecture and providing high surface area as well as abundant coupling contacts for field enhancement. The structural, crystallographic, and optical properties of the resulting DGP substrate were systematically investigated. Using methylene blue (MB) as a probe analyte, the DGP substrate exhibited linear SERS responses under multiple laser excitation wavelengths with detection limits in the low-nanomolar range. Raman mapping and testing across 25 independently fabricated substrates confirmed high spot-to-spot uniformity and batch-to-batch reproducibility. These results demonstrate a simple, cost-effective, scalable, and reagent-economical strategy for producing flexible dendritic gold SERS platforms suitable for on-site SERS-based sensing applications.

Keywords

Cellulose paper, Gold nanostructures, Flexible sensor, Surface-enhance Raman scattering

1 Introduction

Plasmonic materials, particularly noble metals such as gold and silver, have attracted significant attention due to their outstanding optical properties [1]. When reduced to the nanoscale, these materials exhibit distinctive optical behaviors that enable a broad range of multifunctional applications [2]. One of the most notable phenomena is localized surface plasmon resonance (LSPR), which originates from the collective oscillation of conduction electrons on the metal surface under incident light excitation [2]. This effect leads to strong enhancement of the local electromagnetic field around plasmonic nanostructures, significantly amplifying Raman scattering signals. As a result, LSPR plays a crucial role in surface-enhanced Raman scattering (SERS), enabling ultrasensitive, rapid, and label-free identification of chemical and biological analytes [3-5]. Central to SERS performance is the design of plasmonic nanostructures capable of generating intense electromagnetic "hot spots". Among various plasmonic morphologies, dendritic nanostructures, which are characterized by highly branched, hierarchical architectures, have gained increasing attention due to their unparalleled ability to concentrate electromagnetic fields [6]. Their intricate, multi-level branches, and high surface-area-to-volume ratios collectively produce abundant SERS-active sites, often outperforming conventional spherical or smooth nanostructures. These attributes enable dendritic plasmonic substrates to achieve extremely low detection limits and high signal uniformity, making them promising candidates for next-generation SERS sensing platforms.

Despite their advantages, the fabrication of dendritic metal nanostructures remains challenging. Typical synthesis approaches, particularly solution-based methods like electrochemical deposition, galvanic replacement, or chemical reduction, rely on multistep procedures, elevated temperatures, complex surfactants, or slow growth kinetics that limit scalability and reproducibility [7]. Additionally, conventional rigid substrates such as silicon wafers or glass slides restrict the integration of dendritic structures with flexible, low-cost materials [8]. This limitation hinders the practical deployment of SERS

sensors in portable, wearable, or field-deployable applications. Recent advancements, however, highlight a growing trend toward in-situ, solution-based, and template-assisted growth strategies that enable direct formation of complex plasmonic architectures on unconventional substrates [9]. Flexible supports such as cellulose paper offer unique advantages, including high porosity, capillary-driven mass transport, mechanical flexibility, and compatibility with roll-to-roll fabrication, making them ideal platforms for SERS devices intended for point-of-care diagnostics, environmental monitoring, on-site chemical sensing, and food safety evaluation [10]. When dendritic gold nanostructures are grown directly onto cellulose fibers, the resulting three-dimensional network not only increases the active surface area but also enhances photon-matter interactions within the porous matrix, further improving SERS performance. However, the inability to produce large-area, uniform, and mechanically robust dendritic structures through simple and environmentally benign processes remains a major barrier to widespread adoption. In parallel, the field is moving toward one-pot fabrication approaches that simplify synthesis, reduce chemical waste, eliminate the need for post-processing, and improve reproducibility [11, 12]. One-pot in-situ growth of dendritic plasmonic nanostructures is particularly attractive because it merges nucleation, growth, and substrate integration into a single step. This strategy allows precise morphological control while maintaining compatibility with low-cost, flexible, and biodegradable substrates.

Given these advancements, developing a facile, scalable, and substrate-integrated approach for fabricating dendritic gold nanostructures holds significant promise for expanding the practical utility of SERS. In this work, we report a one-pot, in-situ growth of AuNFs directly grown on cellulose paper (DGP) through the direct reduction of Au precursor by hydroxylamine at room temperature for SERS sensing (Fig. 1). Within 24 h, hierarchically branched gold nanostructures nucleate on and interpenetrate the porous cellulose fiber network, producing a dense, three-dimensional forest-like architecture. The substrate exhibited a linear dynamic range, low-nanomolar sensitivity, and excellent spot-to-spot and batch-to-batch reproducibility, underscoring its potential as a cost-effective, flexible, and scalable platform for point-of-care and on-site chemical and biological sensing.

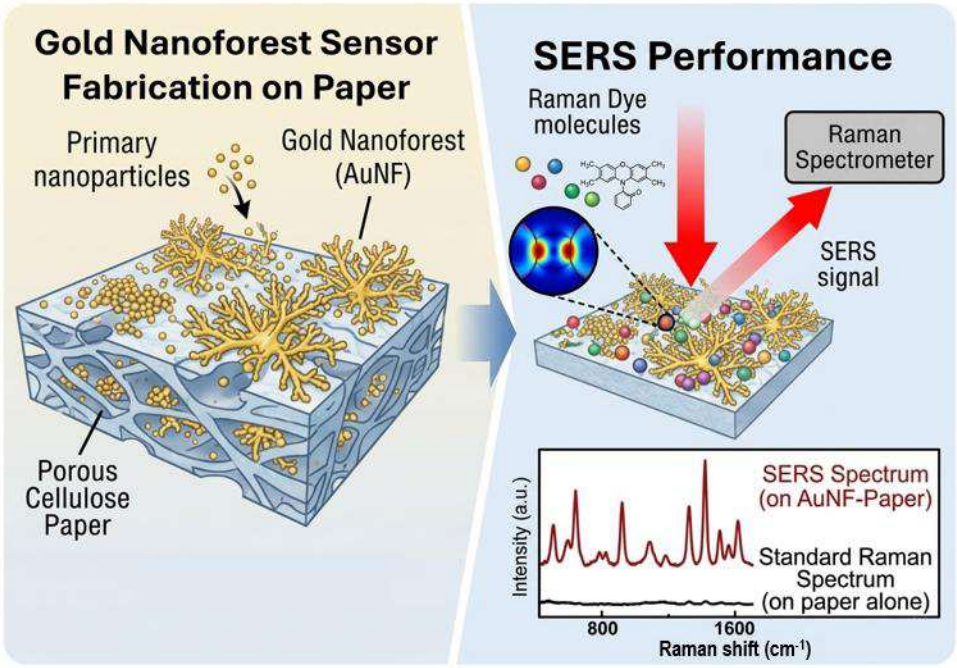


Fig. 1 Schematic illustration of one-pot in-situ growth of dendritic gold nanoforests on paper substrate for SERS sensing.

2 Materials and methods

2.1 Materials

Hydroxylamine (HA), gold chloride hydrate ($HAuCl_4$), and methylene blue (MB) were purchased from Sigma-Aldrich (St. Louis, MO, USA). Cellulose acetate (CA) paper (pore size: 0.45 μm) was purchased from Hyundai Micro Co., LTD (Seoul, South Korea).

2.2 Fabrication of DGP sensor

The DGP sensor was prepared via a simple one-step chemical reduction in solution method. Gold precursor ($HAuCl_4$) solution of 10 mM was quickly added to 50 mM HA solution with 1:1 volume ratio under vigorous vortex. The mixture was then quickly poured onto CA paper placed in a petri dish and kept for 24 h under ambient conditions. After reaction, the substrate was washed with deionized water and dried under ambient conditions.

2.3 Material characterization

Surface morphology was characterized using FESEM (JSM-6700F, JEOL), and the cross-section images and grain structures were captured using TEM (JEM-2200FS with Image Cs-corrector, JEOL). XRD patterns were obtained using an XRD instrument (PANalytical X'Pert Pro). UV–vis absorbance spectra were measured by transferring the AuNF layer from paper to a transparent adhesive film and attaching it at the bottom of a 96-well plate for signal recording using a microplate reader (SpectraMax M2).

2.4 SERS performance

The SERS performance of the DGP sensor was investigated using MB. To determine the limit of detection (LOD) of DGP substrate, 10 μL of MB solutions at various concentrations ranging from 5 nM to 500 nM were dropped on the sensor and dried before Raman measurement. SERS spectra were acquired using a Raman spectrometer Nanoscope systems (NS220 for 633 nm and NS220 for 785 nm, Inc., Daejeon, South Korea) with laser powers and exposure time of 1 mW and 0.2 s for a laser wavelength of 633 nm and 1 mW and 1 s for a laser wavelength of 785 nm, respectively. The LOD value was calculated as $LOD = 3\sigma/S$, where σ is the standard deviation of the background (blank) signal and S is the slope of the linear

calibration curve. The spot-to-spot uniformity of the DGP substrate was evaluated by Raman mapping over a 2000 × 2000 nm area, and the relative standard deviation (RSD) of the SERS intensity at 1620 cm^{-1} was calculated across all mapped points. Batch-to-batch reproducibility was assessed by measuring the SERS response of MB on 25 independently fabricated DGP substrates prepared under identical conditions.

3 Results and discussion

3.1 Fabrication and characterizations of DGP

Dendritic gold nanoforest (AuNF) structures were fabricated via a direct one step reduction using hydroxylamine, as illustrated in Fig. 2. Briefly, as-prepared $HAuCl_4$ and hydroxylamine solutions at a defined concentrations (see Materials and Methods section) were quickly mixed under vigorous vortex mixing and immediately poured onto cellulose acetate (CA) paper substrate, which was left to react for 24 h at room temperature. After washing and drying, the resulting DGP substrate displayed a macroscopically uniform dark coloration across its surface (Fig. 3, inset figure), indicative of extensive and homogeneous Au deposition. Because the nanostructures are grown directly on cellulose paper, whose mechanical flexibility has been demonstrated in our previous paper-based plasmonic sensors [13, 14], the DGP substrate is expected to be compatible with flexible sensing formats. The present study builds on our group's previous development of three-dimensional (3D) plasmonic hierarchical nanostructures for label-free biofluid sensing [15], where we demonstrated that systematic variation of the precursor-to-reducing-agent ratio enables controlled evolution of the nanostructure morphology, with increasing hydroxylamine concentration promoting increasingly dense and branched growth. Dendritic gold nanostructures are themselves well established as SERS-active materials and have been prepared by electrodeposition, galvanic replacement, and wet-chemical reduction [16-18]. However, the properties and performance of dendritic structures are strongly dependent on their synthesis conditions, morphology,

substrate, and integration format. Here, rather than introducing a new structural concept, we examine how this branched architecture can be formed in a single step, directly on a flexible, commercially available CA membrane, using a simple one-pot in-situ growth process, without surfactants or pre-synthesized seeds. A dedicated, quantitative characterization of DGP is therefore essential not only to benchmark its SERS performance in absolute terms, but to establish the structure–property foundation needed to rationally deploy this morphology in the broader range of applications where its distinctive branching, flexible paper-integrated format may offer promising advantages. Thus, this study focuses on the systematic structural characterization and independent validation of the SERS performance of the DGP substrate, providing a fundamental basis for evaluating its potential as a versatile flexible plasmonic platform.

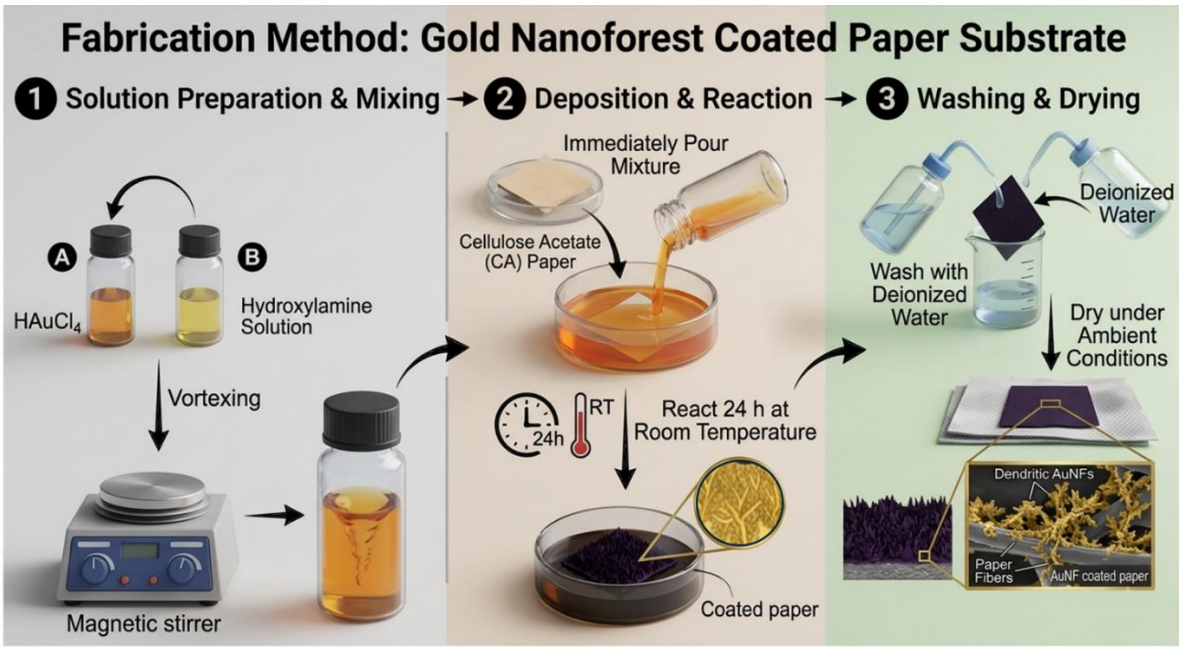


Fig. 2 Schematic overview of the one-pot fabrication process for the DGP substrate: (1) preparation and vortex-mixing of the $HAuCl_4$ and hydroxylamine solutions, (2) immediate deposition of the mixture onto cellulose acetate (CA) paper and reaction for 24 h at room temperature, and (3) washing with deionized water and drying under ambient conditions to yield the dendritic AuNF-coated paper (DGP) substrate.

The surface morphology of the DGP substrate was examined by field emission scanning electron microscopy (FESEM) (Fig. 3). Low-magnification images show that the dendritic AuNFs are densely and uniformly distributed across the paper surface, forming an interconnected, forest-like network with

abundant nanoscale junctions and high-curvature surfaces. This structure is expected to localize and amplify the electromagnetic field at the nanoscale extremities due to the lightning rod effect [19]. At higher magnification, each nanoforest unit is composed of a primary trunk that branches successively into secondary and tertiary fronds, producing a fern-like, hierarchically branched morphology. The terminal branchlets are considerably finer than the primary trunks, giving rise to a broad distribution of local radii of curvature that is expected to support a correspondingly broad distribution of localized electromagnetic hot spots. The hierarchical dendritic morphology can also promote multiple scattering and light trapping between adjacent branches, while variations in branch dimensions and interbranch gaps give rise to broadband plasmonic absorption. These effects result in the strong optical absorption and characteristic dark brown appearance of the DGP substrate [19].

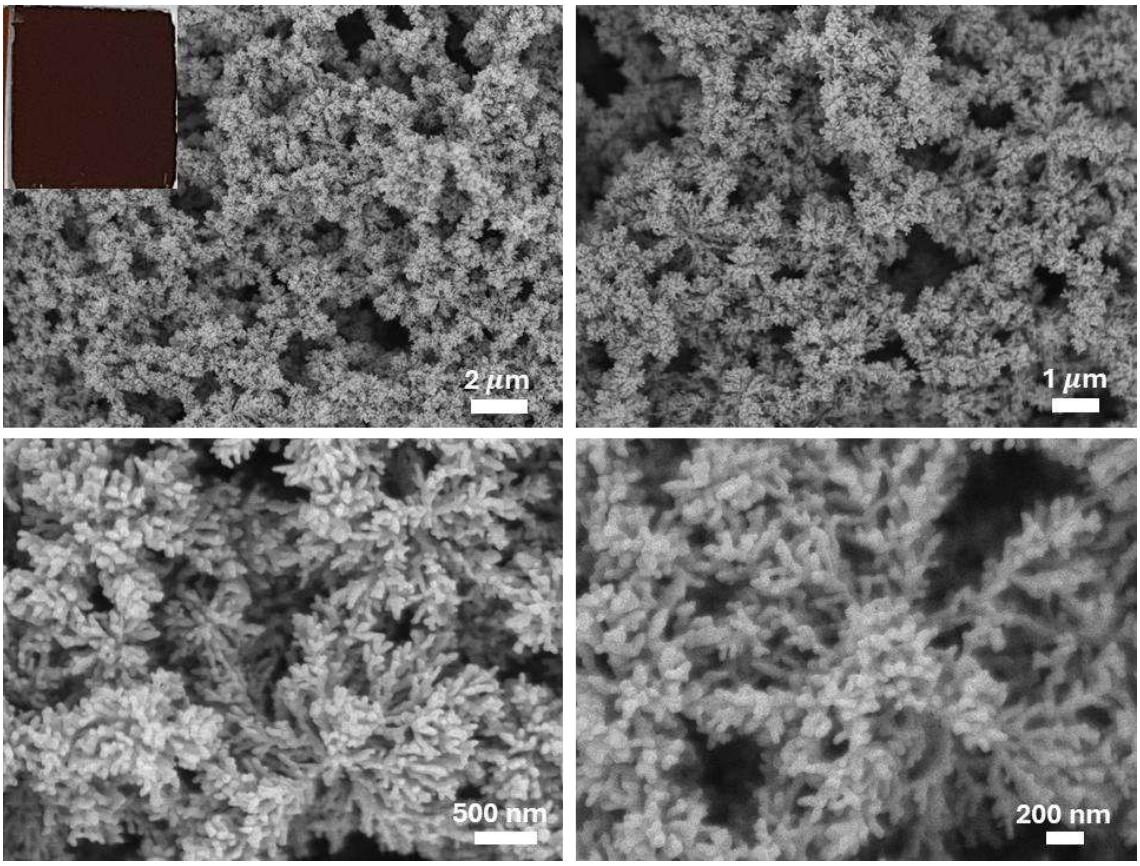


Fig. 3 FESEM images of the DGP substrate at different magnifications, showing densely packed, hierarchically branched dendritic AuNFs uniformly covering the cellulose paper surface; the inset in the top-left panel shows a photograph of the as-prepared DGP substrate.

Detailed nanostructural analysis was performed by transmission electron microscopy (TEM) (Fig. 4). Fig. 4A shows an isolated AuNF unit exhibiting a highly branched, multi-tiered dendritic morphology consistent with the FESEM observations, with primary trunks tapering into progressively finer secondary and tertiary branches. The selected area electron diffraction (SAED) pattern (Fig. 4B) displays spotty diffraction rings that index to the (111), (200), (220), (311), (222), (400), (331), and (420) reflections of face-centered-cubic (fcc) metallic gold, confirming that the AuNFs are polycrystalline [14]. This structure, composed of multigrain boundaries, is expected to exhibit strong surface plasmon absorption and enhanced Raman scattering, which are beneficial for SERS applications [20]. Closer observation of an individual branch tip (Fig. 4C) reveals a porous, granular substructure suggestive of an aggregative growth pathway, in which primary nanoparticles attach and coalesce. High-resolution TEM (Fig. 4D) resolves well-defined lattice fringes with interplanar spacings of approximately 0.23 nm and 0.20 nm, which are assigned to the (111) and (200) planes of fcc gold, respectively. Moreover, the corresponding fast Fourier transform (FFT) pattern (the inset in Fig. 4D) generates discrete reciprocal lattice spots, confirming locally high single-crystallinity within individual branches. Despite the highly complex, porous, and branched overall morphology, the primary AuNF consists of well-crystallized metallic gold, which has been demonstrated for minimizing electron-scattering losses, ensuring strong plasmon oscillation and high SERS enhancement factors [21].

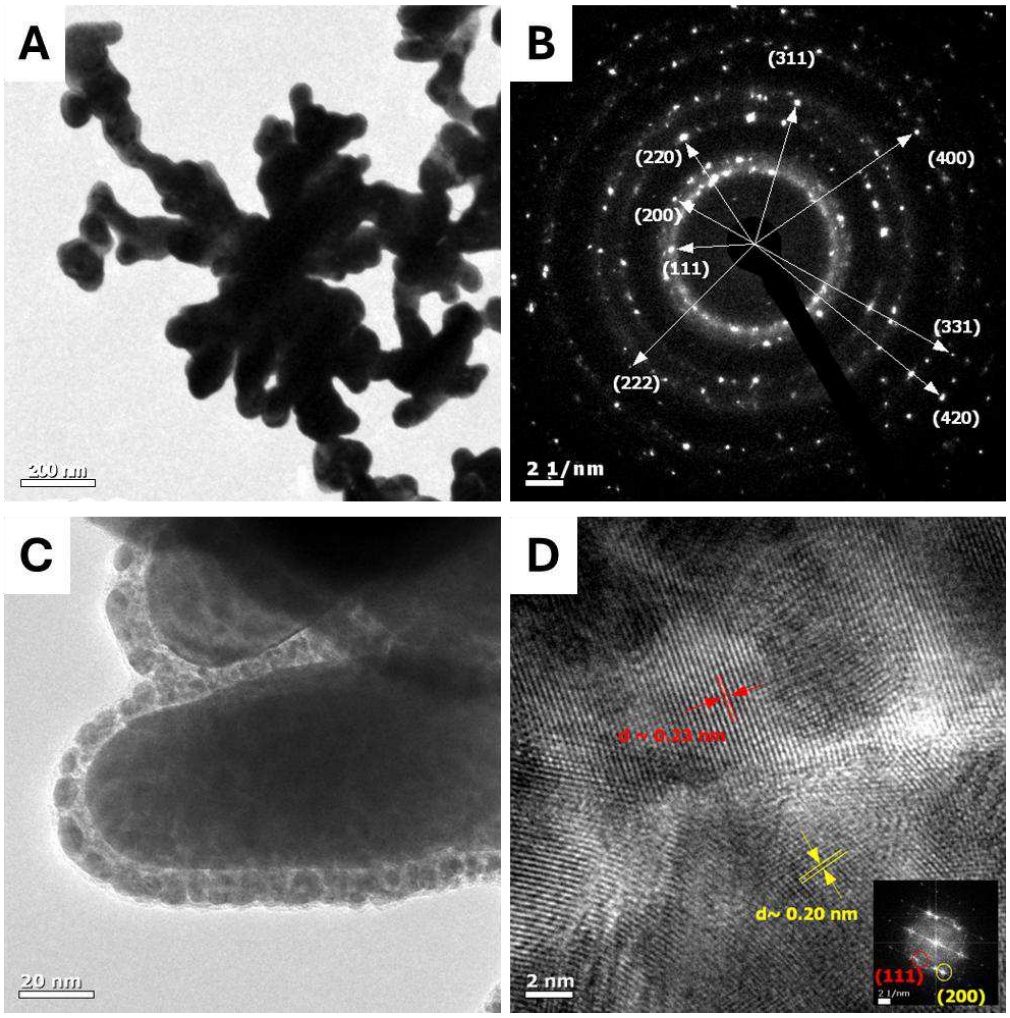


Fig. 4 TEM characterization of the DGP substrate: (A) low-magnification TEM image of an individual dendritic AuNF unit, (B) SAED pattern indexed to the (111), (200), (220), (311), (222), (400), (331), and (420) reflections of face-centered-cubic gold, (C) TEM image of a branch tip, and (D) high-resolution TEM image showing lattice fringes with d-spacings of 0.23 nm and 0.20 nm, corresponding to the (111) and (200) planes, respectively; inset shows the corresponding fast Fourier transform.

The crystal structure of the AuNFs was further verified by X-ray diffraction (XRD) (Fig. 5A). The diffraction pattern exhibits five well-resolved peaks at 38.2°, 44.3°, 64.5°, 77.5°, and 81.7°, indexed to the (111), (200), (220), (311), and (222) planes of fcc metallic gold, respectively, in agreement with the SAED results (Fig. 4B). The pronounced intensity of the (111) reflection relative to the other peaks indicates a preferential (111) crystallographic texture, consistent with the thermodynamically favored low-surface-energy character of this facet [22]. No peaks corresponding to gold oxide or other impurity phases were detected, confirming the phase purity of the as-synthesized AuNFs. The UV-vis absorbance

spectrum of the DGP substrate (Fig. 5B) shows a broad, increasing absorption across the 400–800 nm range without a well-defined localized surface plasmon resonance (LSPR) peak. This featureless, broadband absorption result is characteristic of large, highly anisotropic, and polydisperse plasmonic architectures, in which the variations in branch morphology and inter-branch coupling induce a dense continuum of dipolar and higher order plasmonic modes, suppressing localized resonance peaks [23]. Such broadband absorption is, in fact, advantageous for multi-wavelength SERS applications, as it ensures that the DGP substrate can be efficiently excited across a wide spectral window, particularly the near-infrared (NIR) region for bio-SERS applications [24].

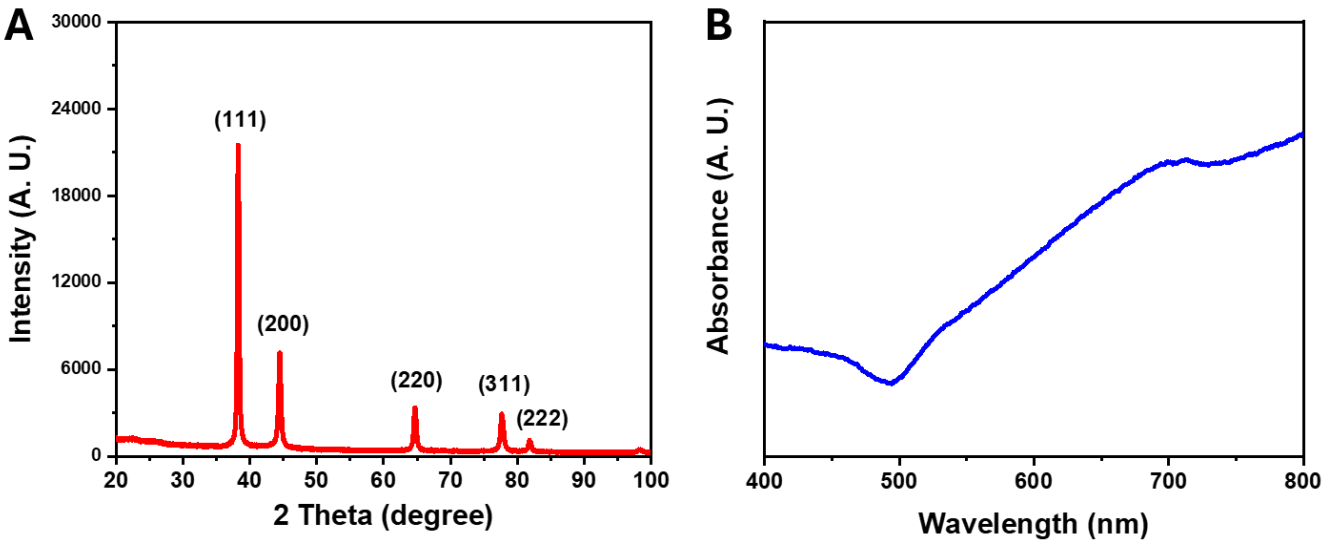


Fig. 5 (A) XRD pattern of the DGP substrate showing diffraction peaks indexed to the (111), (200), (220), (311), and (222) planes of face-centered-cubic gold, and (B) UV-vis absorbance spectrum of the AuNF layer showing a broad absorption across 400–800 nm.

3.2 Mechanism of DGP formation

To rationalize the observed morphology, the proposed growth mechanism of the DGP is depicted in Fig. 6, involving three-stage process: (1) nucleation of primary gold nanoparticles, (2) seed formation onto the porous cellulose fibers, and (3) diffusion-limited dendritic growth. Initially, Au atoms are generated through the reduction of the Au precursor by hydroxylamine. As hydroxylamine is a relatively mild reducing agent, the initial reduction proceeds slowly, causing the Au precursor to spend a prolonged

time in the reaction solution until the concentration of reduced Au atoms reaches the critical supersaturation required for nucleation [25]. During this prolonged pre-nucleation period, positively charged gold ions can interact with the negatively charged carboxylate/hydroxyl functional groups along the CA paper, promoting their adsorption and anchoring onto the porous cellulose fibers. This localized accumulation of Au precursor species provides preferential sites for subsequent reduction and nucleation on the fiber surfaces. These immobilized primary seeds serve as the structural anchor points for the subsequent dendritic growth stages. At early growth stage, because further reduction of gold ions continues to occur preferentially at the surface of the existing seeds rather than through renewed homogeneous nucleation [26], growth proceeds autocatalytically under diffusion-limited conditions. Free gold atoms and small clusters diffuse toward high-energy sites on the primary seeds, with branch growth terminating preferentially in the (111) and (200) facets observed in the HRTEM lattice fringes, producing dendritic clusters. As growth proceeds, adjacent branches interpenetrate and coalesce into progressively more complex, multiply branched architectures, ultimately yielding the dense, interconnected dendritic AuNF network observed by FESEM (Fig. 3). Finally, the hyper-branched dendrites fully cover the fibrous matrix of the cellulose paper, establishing a 3D nanoforest morphology.

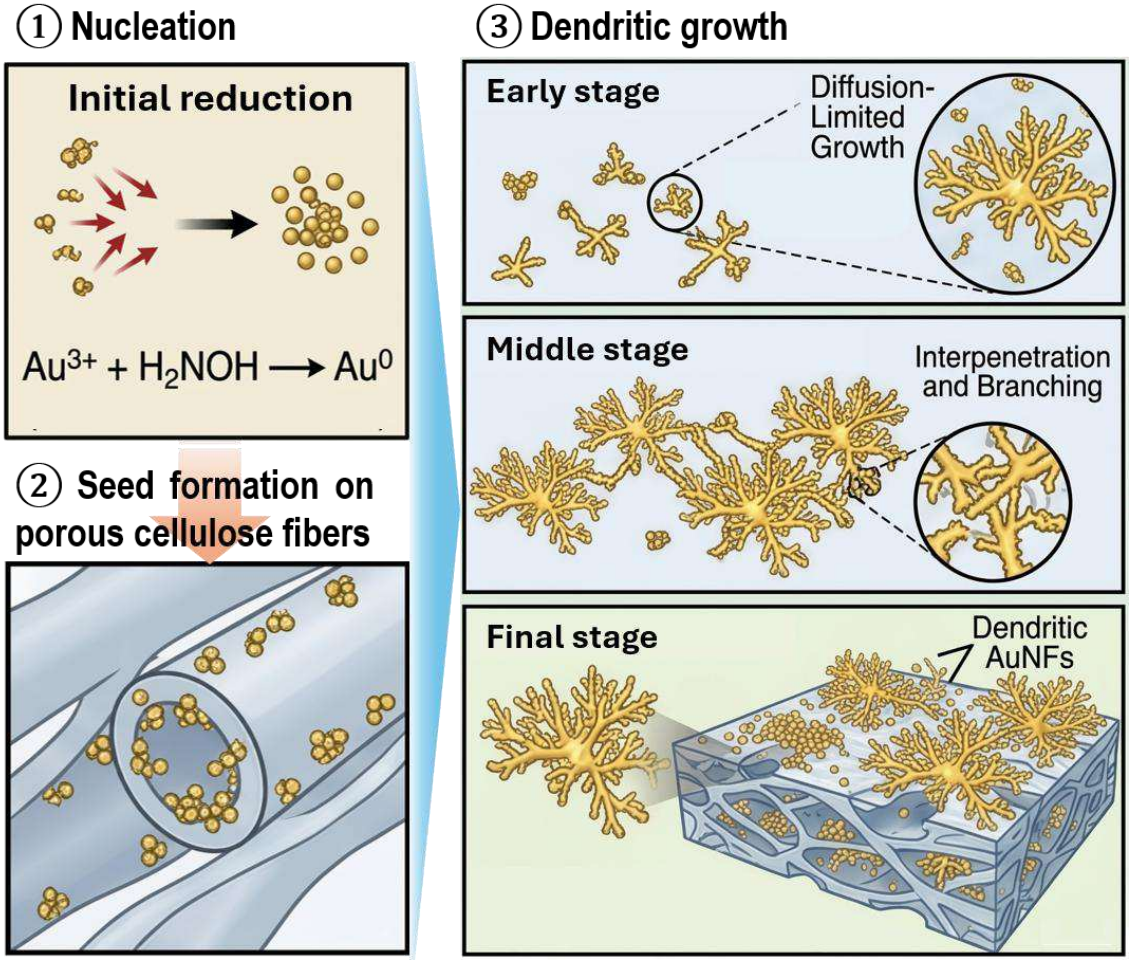


Fig. 6 Proposed growth mechanism of the DGP: (1) nucleation of primary gold nanoparticles via reduction of Au ions by hydroxylamine, (2) seed formation onto the porous cellulose fibers, and (3) diffusion-limited dendritic growth proceeding through early-, middle-, and final-stage branching and interpenetration to form the mature AuNF network.

3.3 SERS performance of DGP

The SERS performance of the DGP substrate was evaluated using MB as a probe analyte under both 633 nm and 785 nm laser excitation (Fig. 7). At both wavelengths, the characteristic vibrational fingerprint of MB was clearly resolved, with the dominant peak at approximately 1620 cm^{-1} assigned to the C-C ring stretching mode [27]. Under 633 nm excitation (Fig. 7A), the SERS intensity decreased systematically with MB concentration across the 100–5 nM range, and the intensity of the 16120 cm^{-1} band exhibited an excellent linear correlation with concentration (Fig. 7B). Under 785 nm excitation (Fig. 7C), a similar concentration-dependent trend was observed across the 500–20 nM range, with a strong linear response

(Fig. 7D). The substantially higher slope obtained at 633 nm results from the resonance matching, as 633 nm aligns closely with MB's electronic absorption band [28]. Based on these calibration curves, the limit of detection (LOD) was calculated to be 143.3 pM at 633 nm and 1.23 nM at 785 nm excitation wavelengths. This low detection limit highlights the high density of accessible electromagnetic hotspots across the DGP network. Moreover, the active response at 785 nm confirms that the broad LSPR profile extends into the NIR region due to the high-aspect-ratio arms, which are advantageous for minimizing auto-fluorescence in complex biological samples.

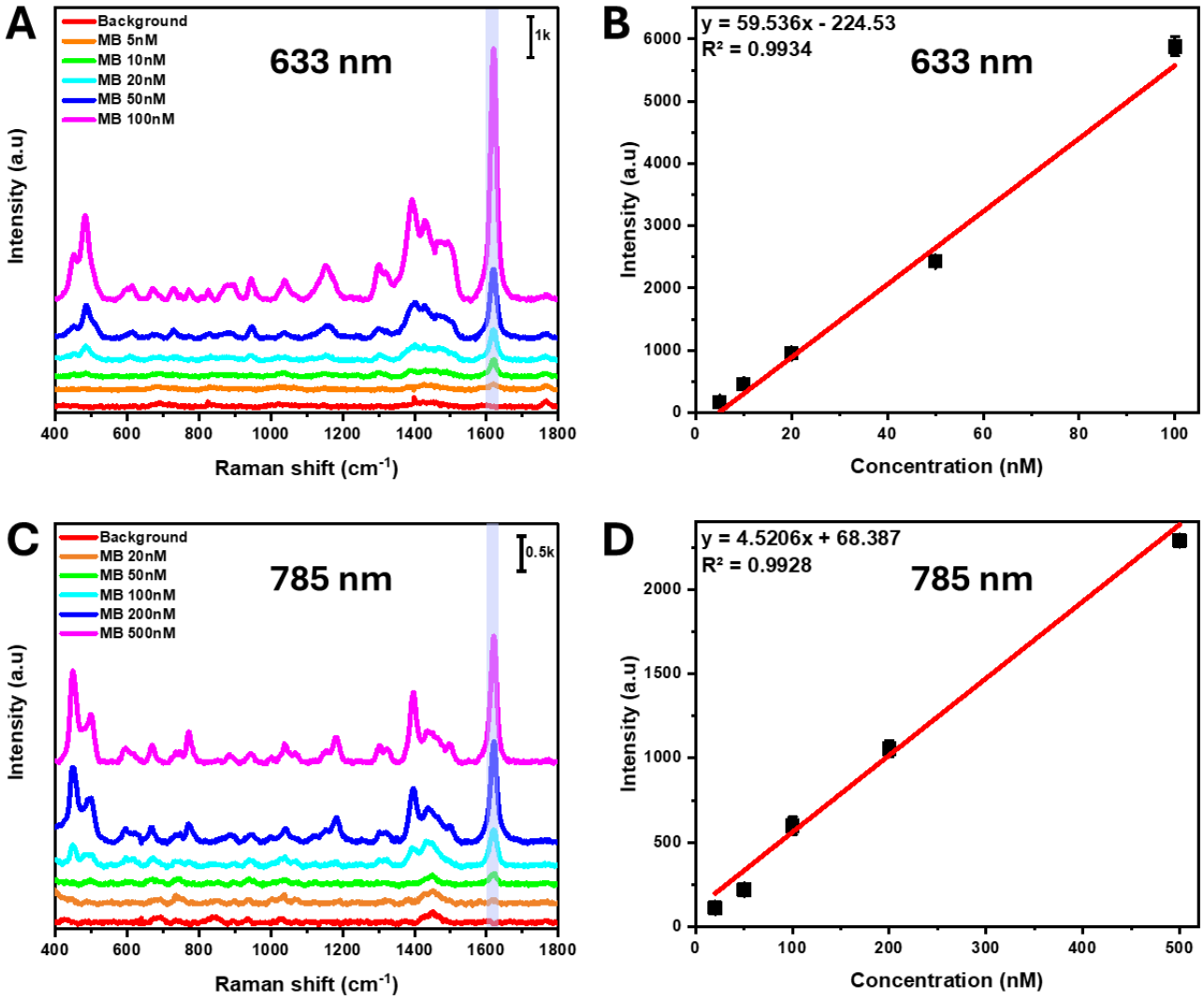


Fig. 7 SERS spectra of methylene blue (MB) on the DGP substrate at (A) 633 nm and (C) 785 nm excitation across the indicated concentration ranges, and the corresponding calibration curves of SERS intensity at 1620 cm^{-1} versus MB concentration at (B) 633 nm and (D) 785 nm.

The uniformity of the DGP substrate was then investigated. Spot-to-spot Raman mapping over a 2000 × 2000 nm area (Fig. 8A, B) yielded relative standard deviations (RSDs) of 6.56% and 6.83% in the intensity of the 1620 cm^{-1} band under 633 and 785 nm excitation wavelengths, respectively, indicating highly uniform hot-spot density across the mapped region. Batch-to-batch reproducibility was further examined by comparing the SERS response across 25 independently fabricated DGP substrates (Fig. 8C, D). The corresponding RSDs of 8.84% (633 nm) and 10.3% (785 nm) confirm the good reproducibility of the one-pot in-situ growth protocol, highlighting its simplicity and effectiveness in generating uniformly distributed plasmonic structures directly on the substrate for consistent SERS enhancement. These results demonstrate that the DGP substrate combines high sensitivity, a wide linear dynamic range, and robust reproducibility, supporting its suitability as a practical, low-cost, and flexible platform for SERS-based molecular sensing.

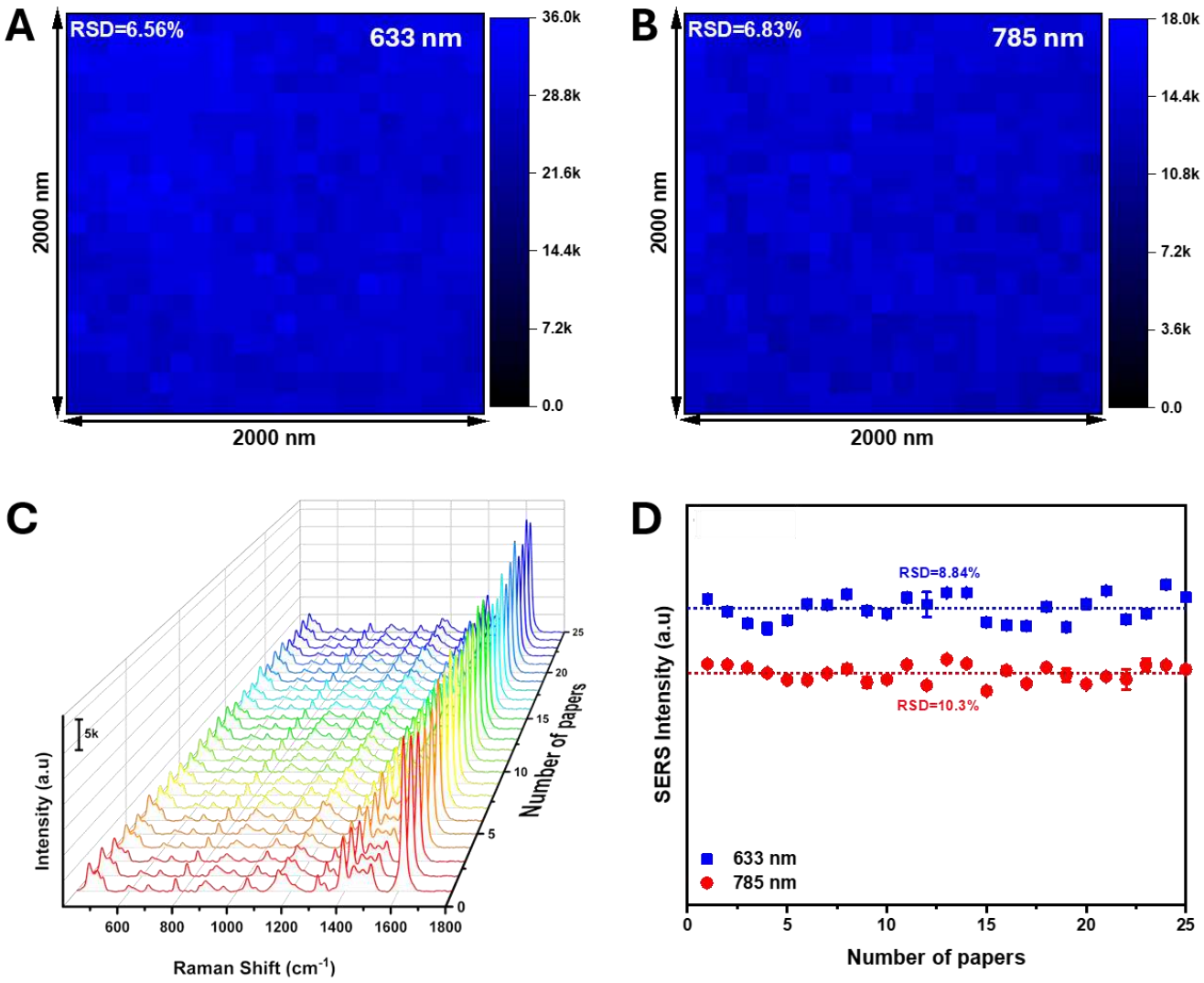


Fig. 8 Uniformity and reproducibility of the DGP substrate: SERS intensity maps of the 1618 cm^{-1} band over a 2000 × 2000 nm area at (A) 633 nm and (B) 785 nm excitation, (C) waterfall plot of SERS spectra collected from 25 independently fabricated DGP substrates, and (D) corresponding SERS intensity at 1620 cm^{-1} across the 25 substrates at 633 nm and 785 nm excitation.

4 Conclusions

We have developed a simple, one-pot, in-situ strategy for growing dendritic AuNFs directly on flexible paper substrate. This surfactant-free approach integrates nucleation, dendritic growth, and substrate functionalization into a single 24-h step, yielding a densely branched, hierarchically structured AuNF network. The resulting DGP substrate exhibits broadband optical absorption across visible and NIR regions, enabling efficient SERS excitation at multiple wavelengths. The DGP substrate achieved a linear

dynamic range with low-nanomolar sensitivity, alongside excellent spot-to-spot uniformity (RSD < 7%) and batch-to-batch (RSD ≤ 10.3%) reproducibility. These attributes, combined with the mechanical flexibility, low cost, and scalability of the underlying paper substrate, position the DGP platform as a promising candidate for point-of-care diagnostics, and wearable-compatible biochemical sensing. Future work will focus on extending this one-pot growth strategy to additional target analytes and complex biological matrices for field applications.

Author contributions

Vo Thi Nhat Linh: Investigation, Validation, Formal analysis, Writing - original draft. Muhammad Shalahuddin Al Ja'farawya: Investigation. Ho Sang Jung: Conceptualization, Methodology, Validation, Project administration, Funding acquisition.

Funding

This research was supported by Culture, Sports and Tourism R&D Program through the Korea Creative Content Agency grant funded by the Ministry of Culture, Sports and Tourism in 2026 (Project Name: Development of Advanced Doping Control Technologies Utilizing Simplified Testing and IoT Integration, Project Number: RS-2026-25546649).

Data availability statement

The data supporting the findings of this research work are available from the corresponding author upon request.

Declarations

Ethics approval and consent to participate

Not applicable.

Consent to publish

Not applicable.

Dual publication

This manuscript is not under consideration for publication elsewhere.

Competing interests

The authors declare no competing interests

References

[1] Kelly KL, Coronado E, Zhao LL, Schatz GC. The Optical Properties of Metal Nanoparticles: The Influence of Size, Shape, and Dielectric Environment. J Phys Chem B. 2003;107(3):668-77. doi: 10.1021/jp026731y.

[2] Willets KA, Van Duyne RP. Localized Surface Plasmon Resonance Spectroscopy and Sensing. Annu Rev Phys Chem. 2007;58:267-97. https://doi.org/10.1146/annurev.physchem.58.032806.104607.

[3] Langer J, Jimenez de Aberasturi D, Aizpurua J, Alvarez-Puebla RA, Auguié B, Baumberg JJ, et al. Present and Future of Surface-Enhanced Raman Scattering. ACS Nano. 2020;14(1):28-117. doi: 10.1021/acsnano.9b04224.

[4] Ja'farawy MSA, Linh VTN, Mun C, Yang J-Y, Kim JY, Park R, et al. Plasmonic Molecular Entrapment for Label-Free Methylated DNA Detection and Machine-Learning Assisted Quantification. Adv Sci. 2025;12(29):2503257. doi: https://doi.org/10.1002/advs.202503257.

[5] Mun C, Linh VTN, Kwon J-D, Jung HS, Kim D-H, Park S-G. Highly Sensitive and Selective Nanogap-Enhanced SERS Sensing Platform. Nanomaterials. 2019;9(4):619. PubMed PMID: doi:10.3390/nano9040619.

[6] Atta S, Beetz M, Fabris L. Understanding the role of $AgNO_3$ concentration and seed morphology in the achievement of tunable shape control in gold nanostars. Nanoscale. 2019;11(6):2946-58. doi: 10.1039/c8nr07615d.

[7] Cardinal MF, Vander Ende E, Hackler RA, McAnally MO, Stair PC, Schatz GC, et al. Expanding applications of SERS through versatile nanomaterials engineering. Chem Soc Rev. 2017;46(13):3886-903. doi: 10.1039/c7cs00207f.

[8] Wang Q, Liu Y, Bai Y, Yao S, Wei Z, Zhang M, et al. Superhydrophobic SERS substrates based on silver dendrite-decorated filter paper for trace detection of nitenpyram. Anal Chim Acta. 2019;1049:170-8. doi: https://doi.org/10.1016/j.aca.2018.10.039.

[9] Zhang L, Liu J, Zhou G, Zhang Z. Controllable In-Situ Growth of Silver Nanoparticles on Filter Paper for Flexible and Highly Sensitive SERS Sensors for Malachite Green Residue Detection. Nanomaterials. 2020;10(5):826. PubMed PMID: doi:10.3390/nano10050826.

[10] Linh VTN, Ja'farawy MSA, Koh EH, Lee M-Y, Park S-G, Kim D-H, et al. Flexible surface-enhanced Raman scattering substrates toward sampling approaches for on-site sensing and diagnosis applications. Appl Spectrosc Rev. 2024;59(1):90-123. doi: 10.1080/05704928.2023.2181818.

[11] Han X, Wang D, Huang J, Liu D, You T. Ultrafast growth of dendritic gold nanostructures and their applications in methanol electro-oxidation and surface-enhanced Raman scattering. J Colloid Interface Sci. 2011;354(2):577-84. doi: https://doi.org/10.1016/j.jcis.2010.11.045.

[12] Liu H, Zhao P, Xiu W, Zhang L, Zhu P, Ge S, et al. SERS paper slip based on 3D dendritic gold nanomaterials coupling with urchin-like nanoparticles for rapid detection of thiram. Sens Actuators B: Chem. 2022;355:131264. doi: https://doi.org/10.1016/j.snb.2021.131264.

[13] Linh VTN, Moon J, Mun C, Devaraj V, Oh J-W, Park S-G, et al. A facile low-cost paper-based SERS substrate for label-free molecular detection. Sens Actuators B: Chem. 2019;291:369-77. doi: https://doi.org/10.1016/j.snb.2019.04.077.

[14] Linh VTN, Kim H, Lee M-Y, Mun J, Kim Y, Jeong B-H, et al. 3D plasmonic hexaplex paper sensor for label-free human saliva sensing and machine learning-assisted early-stage lung cancer screening. Biosens Bioelectron. 2024;244:115779. doi: https://doi.org/10.1016/j.bios.2023.115779.

[15] Linh VTN, Lee M-Y, Mun J, Kim Y, Kim H, Han IW, et al. 3D plasmonic coral nanoarchitecture paper for label-free human urine sensing and deep learning-assisted cancer screening. Biosens Bioelectron. 2023;224:115076. doi: https://doi.org/10.1016/j.bios.2023.115076.

[16] Iost RM, Martins MVA, Crespilho FN. Dendritic Gold Nanoparticles Towards Transparent and Electroactive Electrodes. Anais da Academia Brasileira de Ciências. 2019;91.

[17] Lahiri A, Wen R, Kuimalee S, Kobayashi S-i, Park H. One-step growth of needle and dendritic gold nanostructures on silicon for surface enhanced Raman scattering. CrystEngComm. 2012;14(4):1241-6. doi: 10.1039/c1ce05912b.
[18] Kumari R, Dkhar DS, Mahapatra S, Divya, Singh SP, Chandra P. Nano-Engineered Surface Comprising Metallic Dendrites for Biomolecular Analysis in Clinical Perspective. Biosensors. 2022;12(12):1062. PubMed PMID: doi:10.3390/bios12121062.
[19] Lee HK, Lee YH, Koh CSL, Phan-Quang GC, Han X, Lay CL, et al. Designing surface-enhanced Raman scattering (SERS) platforms beyond hotspot engineering: emerging opportunities in analyte manipulations and hybrid materials. Chem Soc Rev. 2019;48(3):731-56. doi: 10.1039/c7cs00786h.
[20] Zhou C, Yu J, Qin Y, Zheng J. Grain size effects in polycrystalline gold nanoparticles. Nanoscale. 2012;4(14):4228-33. doi: 10.1039/c2nr30212h.
[21] Kusar P, Gruber C, Hohenau A, Krenn JR. Measurement and Reduction of Damping in Plasmonic Nanowires. Nano Lett. 2012;12(2):661-5. doi: 10.1021/nl203452d.
[22] Jung I, Kim J, Lee S, Park W, Park S. Multiple Stepwise Synthetic Pathways toward Complex Plasmonic 2D and 3D Nanoframes for Generation of Electromagnetic Hot Zones in a Single Entity. Acc Chem Res. 2023;56(3):270-83. doi: 10.1021/acs.accounts.2c00670.
[23] Mayer KM, Hafner JH. Localized Surface Plasmon Resonance Sensors. Chem Rev. 2011;111(6):3828-57. doi: 10.1021/cr100313v.
[24] Hang Y, Wang A, Wu N. Plasmonic silver and gold nanoparticles: shape- and structure-modulated plasmonic functionality for point-of-caring sensing, bio-imaging and medical therapy. Chem Soc Rev. 2024;53(6):2932-71. doi: 10.1039/d3cs00793f.
[25] Winkler K, Kaminska A, Wojciechowski T, Holyst R, Fialkowski M. Gold Micro-Flowers: One-Step Fabrication of Efficient, Highly Reproducible Surface-Enhanced Raman Spectroscopy Platform. Plasmonics. 2011;6(4):697-704. doi: 10.1007/s11468-011-9253-0.
[26] You H, Fang J. Particle-mediated nucleation and growth of solution-synthesized metal nanocrystals: A new story beyond the LaMer curve. Nano Today. 2016;11(2):145-67. doi: https://doi.org/10.1016/j.nantod.2016.04.003.
[27] Xiao G-N, Man S-Q. Surface-enhanced Raman scattering of methylene blue adsorbed on cap-shaped silver nanoparticles. Chem Phys Lett. 2007;447(4):305-9. https://doi.org/10.1016/j.cplett.2007.09.045.
[28] Tesema TE, Kafle B, Tadesse MG, Habteyes TG. Plasmon-Enhanced Resonant Excitation and Demethylation of Methylene Blue. J Phys Chem C. 2017;121(13):7421-8. doi: 10.1021/acs.jpcc.7b00864.